https://doi.org/10.3311/PPci.22070

Periodica Polytechnica Civil Engineering, 68(1), pp. 23–36, 2024

Experimental and Numerical Behavior of Basalt Fiber Reinforced Short Concrete Columns Under Axial Loading

Dhiyaa H. Mohammed[1], Adil M. Jabbar[2*], Qais A. Hasan[1]

[1] Civil Engineering Department, University of Technology, 10066, Baghdad, Iraq
[2] Civil Engineering Department, College of Engineering, Wasit University, Wasit, 52001, Al Kut, Iraq
[*] Corresponding author, e-mail: adilmahdi@uowasit.edu.iq

Received: 17 February 2023, Accepted: 14 July 2023, Published online: 16 August 2023

Abstract

This paper presents experimental and numerical investigations to reveal effecting of incorporating basalt fibers into a concrete matrix on the structural behavior and loading capacity of axially loaded short columns. Six volume fractions of chopped basalt fibers are added to the same concrete mixture to prepare six identically reinforced columns. The results illustrate that the bonding forces between microfilaments and matrix increase to provide good internal confinement for concrete ingredients, which enhances compressive strength and column loading capacity. The 0.3% basalt fiber awarded the best compressive strength, while 0.15% and 0.3% awarded the best load capacity to the column. The Addition of basalt fibers delays cracking to increase the cracking load by about 50% more than no fiber column, which indicates that it needs more energy to overcome the bonding strength between filaments and matrix. At the ultimate state, the loading capacity increases by 15% and 17% for 0.15% and 0.3% of basalt fibers and by 10% and 12% for 0.45% and 0.6% of basalt fiber. The 0.75% decreased compressive strength by about 6% but raised the column's ultimate load by 18%. Therefore, basalt fiber benefits the cracking load more than the maximum load. The finite element showed approaching the peak load in numerical and experimental results. The longitudinal rebars and ties do not yield at the ultimate state. Increasing the reinforcement ratio raises loading capacity while lowering the yield stress of bars minimizes the maximum load.

Keywords

basalt fibers, short column, compressive strength, bearing capacity

1 Introduction

Reinforced concrete (RC) short columns are prime components in RC structures. Short columns represent a supporting element for other structural members. They are utilized in bridge piers, building skeletons, and other concrete structures. Columns' loading capacity and durability are essential to the safety, applicability, and economy of the whole structure. Nowadays, there is effectiveness at enhancing the mechanical properties of concrete by merging different types of fibers with concrete matrices, such as steel fibers [1], glass fibers [2], synthetic fibers [3, 4], carbon fibers [5], polyvinyl alcohol fibers [6], and basalt fibers [7]. That is mainly because the suitable volume contents and fiber properties and length can effectively merge with the weak matrix in concrete to adequately restrain the expansion of internal cracks in concrete and then enhance the mechanical properties of concrete.

Generally, numerous types of fiber-reinforced concrete have different effects on mechanical properties or application features. For instance, adding steel fiber to concrete can enhance energy absorption and tensile strength, but steel fiber cannot resist corrosion. Adding glass fiber into concrete can improve energy absorption, but its resistance declines in the long term. Although carbon fibers attribute to hardness and high strength, their cost is high [8]. Due to the above issues, basalt fiber is significantly researched since it has high tensile strength, corrosion resistance, suitable chemical soundness, no environmental effects, and no pollution [9]. Therefore, it is insistent to investigate the mechanical properties of basalt-fiber-reinforced concrete (BRFC) and the related concrete members.

Basalt fiber is a new type of natural fiber having a chemical composition similar to glass fibers, silicates account for approximately 50% of its composition, but it has higher strength and higher resistance to alkali, acid, and salt attacks [10–13]. These features put it in a promising rank to use in concrete mixtures to enhance some mechanical properties. Basalt fibers have produced in several shapes and lengths. They can be found as chopped fibers, filaments,

Cite this article as: Mohammed D. H., Jabbar, A. M., Hasan, Q. A. "Experimental and Numerical Behavior of Basalt Fiber Reinforced Short Concrete Columns Under Axial Loading", Periodica Polytechnica Civil Engineering, 68(1), pp. 23–36, 2024. https://doi.org/10.3311/PPci.22070

or minibars of fine filaments collection glued together by epoxy resin [11, 14]. Chopped basalt fibers have been used in many studies to clarify their effects on concrete properties. Branston et al. [15] found that adding basalt fiber to the concrete mix at (0.3–0.5)% by volume can increase its strength, while above 0.5%, it will be detrimental to concrete strength. Ayub et al. [16] specified 1% basalt fiber content as the optimal ratio. However, the benefits dosage of basalt fibers is less than that of steel fibers, it was found that adding 12 kg of chopped basalt fibers to 1 m^3 of concrete can enhance its flexural strength at the same level of increasing it when using 40 kg/m^3 of steel fibers [15].

Adding basalt fibers to the concrete ensures micro-reinforcement of the mixture in the three directions and obstructs micro-cracks [17, 18]. Information indicates that using 3 kg/m^3 of basalt fibers in concrete increases the tensile strength by 29%, while adding 25–45 kg/m^3 of steel fibers increases the tensile strength by only 12–17% in normal-strength concrete (NSC). On the other hand, using 0.9 kg of basalt fibers per 1 m^3 of cement mortar can raise tensile strength by 49% and compressive strength by 58% [17].

The impact of basalt fiber on the mechanical properties of concrete depends on the added volumetric ratio. Borhan [19] determined 0.3% of basalt fibers in NSC confer the best compressive strength, whereas 0.5% decreased it. Dias and Thaumaturgo [20] found that 0.5% and 1.0% of basalt fibers decreased compressive strength by 4.5% and 36%. El-Din et al. [21] detected that using 18 kg/m^3 (0.64% by volume) of basalt fibers promoted compressive strength by 15%. El-Gelani et al. [22] found that 1.8 kg/m^3 of basalt fibers increased the compressive strength by 5.7% at a 28-day test and the flexural strength by 16.5%. Revade and Dharane [23] stated that incorporating basalt fibers into NSC at 1.0%, 1.5%, and 2.0% by weight of cement raised the compressive strength by 13.2%, 11.8%, and 10%, respectively, and splitting tensile strength by 11.3%, 17.4%, and 20.8%, respectively. Galishnikova et al. [24] stated that the compressive strength of HSC was not affected by increasing chopped basalt fiber content. Abdulhadi [25] explored basalt fibers' effect on the strength of 30 MPa NSC. The author used 0.3%, 0.6%, 0.9%, and 1.2% basalt fibers in a concrete mix. The results presented that the added fibers minimized compressive strength. However, 0.3% and 0.6% of basalt fibers promoted tensile strength by 2.6% and 22.9%, while 0.9% and 1.2% decreased the splitting tensile strength by 11.3% and 19.8%. Krassowska and Kosior-Kazberuk [26] used 50 mm length basalt fibers at 2.5 and 5 kg/m^3. The results showed that adding basalt fibers raised compressive strength by 4.76% and 0.99% and splitting tensile strength by 10.06% and 16.39%, respectively.

It is also shown that the water content in the mixture has a co-effect on compressive strength, where Algin et al. [27] searched the influence of basalt fibers on the mechanical properties and workability of two w/c ratios of normal concrete. The results indicated that the slump decreased with increasing basalt fiber content. A slight increase in compressive strength occurred upon increasing basalt fiber from 0% to 0.8%. At 0.8% basalt fiber, an increase of 16% and 10% in compressive strength for w/c ratio of 0.59 and 0.47, respectively, while splitting tensile strength increased by 34% and 26% for the same w/c ratios. Al-Kharabsheh et al. [28] showed that lowering slump with increasing basalt fiber content. The authors attributed the decrease in workability to the adsorption of mixing water by basalt fibers and the increase in surface area due to its small diameter. Increased surface area required more mortar to facilitate sliding. However, a large surface area can increase the viscosity of concrete. On the other hand, the authors suggested that increasing basalt fiber content could raise air voids and lower the unit weight of concrete [29]. Therefore, adding a superplasticizer is advised to reduce air voids.

Several studies have shown an increase in compressive strength when basalt fiber content is increased up to 1.5%. However, this increase is uneven, and no precise explanations were given for the reasons. Ramesh and Eswari [8] showed that slight increment in compressive strength upon adding basalt fiber at 1.5%, while 2% content decreased it. They attributed the reason for lowering compressive strength at 2% content to the weak bond between the concrete and the basalt fibers. Therefore, they concluded that the excess percentage of basalt fibers will not bond with the matrix and generates additional voids that make them points for stress concentration causing brittle failure. Another research by Meyyappan and Carmichael [30] studied the variety of basalt fiber's effect between the ages of 7 and 28 days on specimens. They used 0.5%, 1.0%, 1.5%, 2.0%, 2.5%, and 3.0% basalt fibers in M30 concrete. The results showed an increase in compressive strength at the age of 7 days by 55-64% compared to the strength at 28 days. However, their results showed raising the compressive strength by 11.45% at a 1.0% ratio of basalt fiber, while at 3.0% content, the compressive strength decreased by 33.87%.

Short columns have high stiffness that tempts most of the force acting on a building. The inappropriate design of short columns to support these loads may lead to damage and shear failure. The behavior of the short column under extreme load is known as the short-column effect. Therefore, Special attention is needed for short column design, especially for earthquake-prone areas. The failure of a short column is catastrophic as they undergo brittle shear failure. Consequently, different methods are tried to enhance the short column strength. One of these methods is increasing its capacity by incorporating fibers in the concrete constituted to minimize brittle failure [31].

Several researchers have searched basalt fiber's influence on the mechanical properties of concrete, and others focused on the impact of basalt fibers on the structural behavior of concrete beams. Jabbar et al. [32] found that adding basalt fibers to ultra-high-performance concrete can delay the first cracking load and enhance compressive strength in beams. Wang and Zhang [33] also found that adding basalt fiber can restrict the expansion of flexural cracks in beams. However, few studies focused on the influence of basalt fiber on the loading capacity of short columns. The use of basalt fibers as micro-reinforcement for short concrete columns was tested by Wang et al. [34]. The authors tested the suitable length and concluded that the 12–24 mm chopped basalt fibers were the optimal lengths to arrive at the best compressive strength, and 0.15% basalt fiber content is the best volume fraction. Wang et al. showed that adding basalt fiber at 0.15% enhanced the loading capacity of short columns by 28% for 12 mm and 20% for 18 mm long. Wang et al. [35] found that using a 0.15% ratio of basalt fiber could enhance the loading capacity of a spirally reinforced short column by about (28–29.5)%.

Since basalt fibers have enhanced compressive strength, this research aims to investigate the effect of their addition to concrete on the loading capacity and the structural behavior of short columns to reach the best volume fraction. Six volume fractions of basalt fibers were experimentally investigated for concrete compressive strength and structural behavior of short columns. Loading at the first crack and ultimate state with corresponding longitudinal displacements were discussed. The study was completed by conducting a finite element analysis (FEA) to investigate the column structural behavior, the stresses in longitudinal bars and ties, and the effect of changing reinforcement ratio with yield stress on the loading of the columns.

2 Experimental investigation

2.1 Column specimens

Six identical circular section short columns were prepared for the test. The column had a diameter of 150 mm and a length of 750 mm. The slenderness ratio was 5, which was less than 12. It was longitudinally reinforced by 4 bars of 8 mm diameter and transversely by 5.5 mm diameter ties. The tie-spacing was constant at 120 mm, as shown in Figs. 1 and 2. A concrete cover of 20 mm was provided. The reinforcement ratio was 1.13% for all columns.

The spacing between ties was specified according to the ACI 318-19 [36] requirements. The physical properties of steel rebars are listed in Table 1.

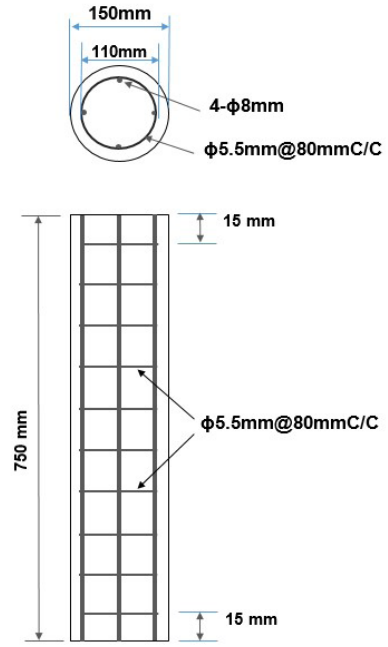

Fig. 1 Short column details

Fig. 2 Details of rebars used to reinforce the columns

Table 1 Mechanical properties of steel rebars used in experiments

Nominal diameter, mm	Actual diameter, mm	Area of the rebar, mm^2	Yield stress, *fy*, MPa	Ultimate strength, *fu*, MPa	Modulus of elasticity, E_s, GPa	Maximum elongation, %
8	7.954	49.69	563	624	200	7.678
5.5	5.100	20.43	394	443	200	1.192

2.2 Material properties and mix proportion

An identical mix was used for all columns. The difference was in chopped basalt fiber content and high-range water reducer admixture (HRWRA) dosages. A mix proportion included 430 kg/m^3 of ordinary Portland cement (ASTM Type I), an 823 kg/m^3 natural fine aggregate with a 2.75 fineness modulus and compacted density of 1656 kg/m^3, and 847 kg/m^3 crushed natural gravel with a maximum size of 14 mm and compacted density of 1527 kg/m^3, which was used as coarse aggregate. Water content was 215 kg/m^3 to award a 0.5 water-to-cement ratio. Five basalt fiber percentages were added to the identical concrete mixture as a volume fraction: 0.15%, 0.30%, 0.45%, 0.6%, and 0.75%, besides one without fibers as a reference mix. Therefore, six mixtures were used to cast six columns. The water-to-cement ratio was kept constant at 0.5. During the experimental mixtures, it was found that the workability of concrete decreased with increasing basalt fiber content. To modify the workability, a superplasticizer of type Sika Viscocrete-180G was added in increasing doses with increasing fiber content by a ratio of 0.4%, 0.6%, 0.8%, 1.0%, and 1.25% of cement weight. Sika Viscocrete-180G is a high-range water reducer and super plasticizing admixture with a polycarboxylates polymer base [37]. Chopped basalt fiber has a (16–18) μm diameter and a 12 mm length. It was as filaments collected together in slices. The tensile strength of the solo filament is 1500 MPa, and the density of basalt fiber equals 2800 kg/m^3 [17].

The prepared mixture was poured into the column mold and compacted with a 16 mm steel rounded end rod to ensure that the concrete reached all parts inside the mold. Three or more cylinders with (100 × 200) mm size were also cast from the same mixture as control specimens for testing cylinder compressive strength, as shown in Fig. 3.

All specimens were entirely covered by polyethylene sheet to prevent water evaporation. Twenty-four hours after casting, the specimens were de-molded, then cured in water at 23 ± 2 ºC for 28 days. One day before testing, the specimens were taken out of the water and left to dry to examine in a saturated, dry surface condition.

2.3 Test setup and instrumentation

A compression bear load was subjected to the top section of the column. Two steel bolsters representing bases support the column from top and bottom. They were made of a steel ring of a diameter slightly larger than the column diameter. The bolsters were used to install the column in the testing device, as shown in Fig. 4. Rubber pads having a diameter of 150 mm and a thickness of 5 mm were placed

(a) (b)

Fig. 3 (a) Casting concrete into the mold, (b) columns after demolding

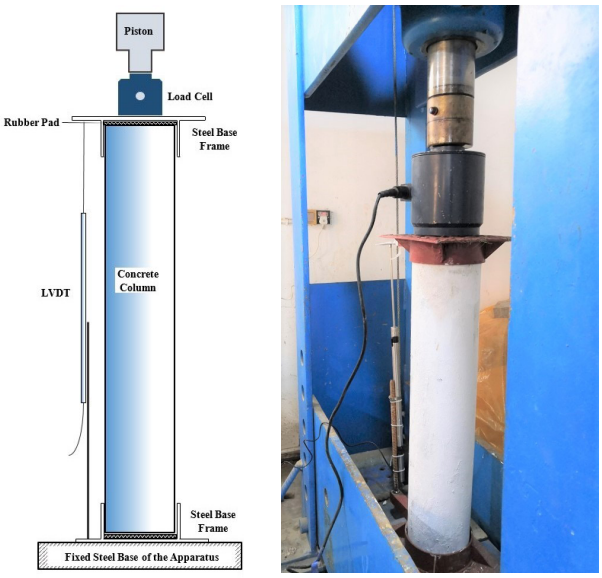

(a) (b)

Fig. 4 Loading system for short columns

between the base of the bolsters and the concrete column at the top and bottom to avoid the impact load. A universal testing machine of 1000 kN capacity was applied to test the columns.

A load cell of 1000 kN capacity was placed over the upper steel bolster to record the load increment. An LVDT tool was placed between the upper and lower bolsters to record the axial displacement. The toots have access to a Data Logger to record the readings successively during the test.

For (100 × 200)mm concrete cylinder specimens, a Matest compressive testing device of 2500 kN capacity was used, as shown in Fig. 5. All columns and control specimens were tested at 28-day ages.

Fig. 5 Testing of control specimens for compressive strength

3 Experimental results and discussions

The examination included testing the devices used to record the load and displacement, which was done by pre-loading each specimen by 40 kN and kept for 3 minutes to notice the reliability of the loading and measuring system. The actual loading was subsequently started with gradation loads. The columns were loaded by 40 kN per grade up to 160 kN, then by 20 kN until failure. Each load increment was kept for 2 minutes. The loading system is shown in Fig. 4.

The tested short columns exhibited an ability to bear more than half of the failure load before the first crack occurred. The loading ability increased when basalt fibers were added to the concrete matrix to reach three-quarters of the failure load. The column continued to bear loading even after falling the concrete cover. After the peak, the column also continued to carry loading despite the load dropping gradually but never less than 40% of the column's ultimate load, which refers to ductility acquired by the column upon adding basalt fibers because of gradually de-bonding them from the matrix.

3.1 Test results of compressive and tensile strength

For compressive and splitting tensile strength, three or more concrete cylinder specimens of (100 × 200) mm were tested per every basalt fiber content at 28 days for each strength, and the average value was considered. Test results are listed in Table 2.

Increasing basalt fiber content up to 0.6% raised the compressive strength, while the 0.75% content caused decreasing compressive strength by 5.92%. The percentage of increment of compressive strength increased up to 0.3% basalt fiber content, which awards a higher increment, then decreased after 0.3% content, as illustrated in Table 2.

The lower the content of basalt fibers, the higher the increment in splitting tensile strength. 0.15% and 0.30% of basalt fibers are the best content that raised the tensile strength more than the other volume fractions. Both percentages increase tensile strength by about 36% over non-fiber concrete. However, 0.75% awards the lower increment in tensile strength.

Basalt fiber is a microfilament that has a 16–18 μm diameter. Even when its content is small, it gives plenty of filaments. The low percentage of basalt fiber could distribute in all directions within the concrete matrix. And because of its micro diameter, the bonding strength between the

Table 2 Cylinder compressive strength per basalt fiber content

BF content %	f_c', MPa	PoV of f_c', %	SD	COV	*fspt*, MPa	PoV of fspt, %	COV
0.00	32.42	--	1.52	0.047	3.61	0.00	0.031
0.15	38.87	19.90	1.45	0.037	4.92	36.29	0.005
0.30	40.10	23.69	1.09	0.027	4.90	35.73	0.003
0.45	37.20	14.74	0.50	0.013	4.62	27.98	0.005
0.60	35.46	9.38	1.35	0.038	4.28	18.56	0.004
0.75	30.50	-5.92	1.21	0.040	4.04	11.91	0.008

f_c' = cylinder compressive strength, PoV= Percentage of variation, *fspt* = Splitting tensile strength, COV = Coefficient of variation

filament and concrete increases, giving high internal confinement and reducing the early shrinkage. These features enhanced compressive strength.

When the percentage expands over 0.3%, the number of filaments increases, then large numbers of filaments accumulate and warp because of their flexibility to form small balls in which mortar is trapped. The number of balls increases with a further increase in basalt fiber content. The straight-distributed filaments contribute to raising the strength, while the twisted and balled ones act as voids inside the concrete microstructure to concentrate the stresses and lead to a relative decrease in the strength.

It can be considered that 0.3% of basalt fiber is the best volume fraction to enhance compressive strength among the five ratios adopted in this study. However, the lower percentages of basalt fibers award better results for compressive strength than higher percentages in the small specimens.

3.2 BFRC short column results

Test results of short columns are listed in Table 3. Basalt fiber percentages up to 0.6% increase the ultimate loading capacity of the short columns, while 0.75% content reduces it by 9%. Adding basalt fibers to the concrete matrix at 0.15% and 0.3% raises the load-bearing capacity of the columns by 17% and 15%, respectively. The 0.45% and 0.6% increase the column ultimate bearing by a lower percentage: 12% and 8%, respectively, as illustrated in Table 3.

At the first cracking stage, the addition of basalt fibers contributes to delaying the initial cracking and raises the loading capacity by about 50% more than the no-fiber concrete column at 0.6% basalt fiber content and lower. However, for 0.75% basalt fiber content, the first cracking load raises only by 18%, as illustrated in Fig. 6.

The results show that basalt fibers have beneficial to the first cracking load more than that to the ultimate loading of the short columns due to the relatively high bonding strength between basalt filaments and concrete matrix, which needs more energy to overcome the bond.

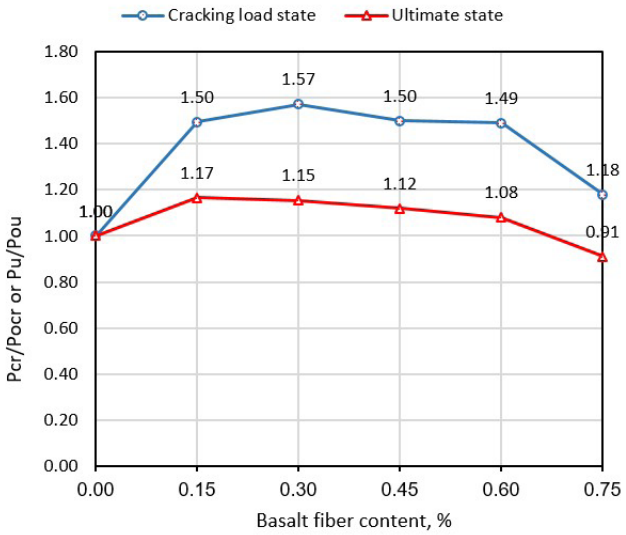

Fig. 6 The loading capacity of short columns at cracking and peak state for different basalt fiber content

The chopped microfilaments of basalt fibers can be well combined with the concrete matrix to form a spatial network. That network can improve the combination of concrete constituents, including cement paste to coarse aggregate. The spatial network encases the coarse aggregate and acts as a hindrance to aggregate movement during compression, which can enhance the properties of an interfacial transition zone between coarse aggregate and cement paste. Thus, basalt fiber can provide peripheral restraint to withstand the transverse expansion upon applying compressive stresses on the specimen. Accordingly, basalt fibers' presence can prevent a generation of a large number of micro cracks and discontinuity of the existing ones. That makes the erection and evolution of cracks need more energy to beat the relatively high bonding forces when compression is applied to a specimen. The regular arrangement of the fibers within the concrete microstructure contributes to this behavior by better effectiveness. Therefore, the loading capacity of the BFRC short column is significantly improved, and the initial cracking is delayed.

Table 3 Short columns' results at first cracking and peak states

Column ID	f_c' MPa	Cracking load *Pcr.*, kN	Δ*cr.* mm	Ultimate load *Pu*, kN	Ultimate displacement Δ*u*, mm	*Pcr*/ *Pu*	*Pcr*/ *Pcro*	*Pu*/ *Puo*
CS120-0.00	32.42	258.89	1.86	461.64	3.0	0.56	1.00	1.00
CS120-0.15	38.87	387.77	1.08	538.57	3.5	0.72	1.50	1.17
CS120-0.30	40.10	406.87	1.22	532.73	3.6	0.76	1.57	1.15
CS120-0.45	37.20	388.70	1.28	516.65	3.2	0.75	1.50	1.12
CS120-0.60	35.46	386.02	1.34	498.73	3.7	0.77	1.49	1.08
CS120-0.75	30.50	305.60	1.44	420.70	2.7	0.73	1.18	0.91

The behavior of BFRC has been interpreted as follows: Before the extension of cracks in the concrete matrix resulting from the loads or external influences, the random spread of basalt fibers contributes to enhancing the internal confinement of the concrete matrix, which raises the load before cracking. When the loading reaches sufficient energy to overcome the bond strength between microfibers and concrete matrix, the cracks begin to extend. That happens after overcoming the bonding strength. On the other hand, the relatively strong bond between microfibers and the matrix hinders the progression of cracks and acts to bridge the adjacent parts of the crack to award concrete with ductility. The failure occurs upon the withdrawal of all the filaments along the sides of the crack.

On the other hand, the presence of steel ties with the basalt fibers improves the ductility of the short column after the peak state due to the high energy required to overcome the bonding force of the huge number of fine filaments of basalt fiber.

3.3 Effect of basalt fibers on compressive strength and loading capacity of columns

The percentage of increment in small specimens is more pronounced than in larger ones at 28 days, where the addition of basalt fibers has a higher impact on the compressive strength of small-sized cylinders than on the longer columns, as shown in Fig. 7. The internal confinement caused by basalt fibers, in addition to the external confinement represented by the small size due to the geometry of the cylinder (height-to-diameter ratio equals 2.0) compared to the large size of the column resulted from the geometry (height-to-diameter ratio equals 5.0), contributes to increasing its effect on the compressive strength of small concrete cylinders. Also, the control of working on small specimens is better than on the relatively larger specimens of columns with rebars. However, basalt fiber's effect on the cracking load of short columns is the greatest because of the high bonding force between the microfilaments and the matrix, which needs more energy to overcome the bonding forces. In any case, increasing the cracking load more than the maximum bearing load inversely affects the structural behavior of the column because of the approaching between them. So, it will not give an early indication of the possibility of failure. On the other hand, incorporating basalt fibers into the concrete matrix award more durability and ductility.

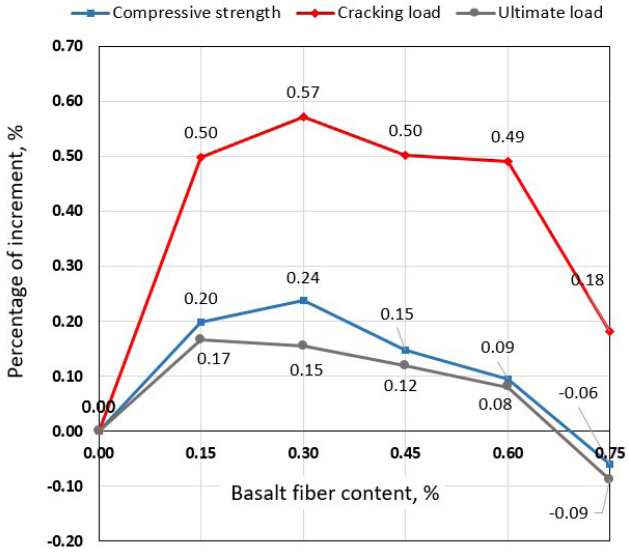

Fig. 7 Relationship between basalt fiber content and cylinder compressive strength, cracking load, and ultimate load of short columns

3.4 Failure mode of columns

During the test, vertical cracks occurred before column failure near supports. Upon increasing the load, the cracks developed gradually in number and width, then the concrete was crushed, and the column failed. However, the steel ties remained sound when the columns were damaged. All the columns failed due to the crushing of concrete at the upper or lower third or both ends near the supporting bolsters, as illustrated in Fig. 8. That was because the stresses were concentrated near the loading point and the longitudinal bars did not yield. At failure, the cracks propagated longitudinally and focused near the supporting bolsters.

The cracks propagated to the mid-length in column CS120-0.3 and the concrete cover fell, while in column CS120-0.15, the cracks extended to near the middle without the concrete cover falling. These columns experienced the highest load capacity. Generally, BFRC short columns were cracked later than the non-fibrous columns. According to the crack pattern of columns, the

Fig. 8 Failure patterns of short columns

bearing region of the column needs to be strengthened and increased its confinement to allow the load to move to the other parts of a column and increase its loading capacity.

4 Numerical analysis of columns

A numerical analysis was developed in the Abaqus software to trace the structural behavior of columns under axial compressive loading. The finite element analysis (FEA) was performed by displacement control to capture the load at each increment.

4.1 Numerical simulation of columns

The tested specimen consists of a concrete column with a circular section, longitudinal rebars of 8 mm diameter, transverse ties of 5.1 mm diameter, and supporting steel bolsters. The concrete column and steel bolster are discretized with a 3-dimensional continuum that has 8 nodes with reduced integration (C3D8R). Steel rebars are discretized by 2 nodded link elements (T3D2). C3D8R elements have 8 nodes with 3 degrees of freedom per node. This element can model solids in 3 dimensions with or without reinforcement. It can consider tensile cracking, compressive crushing, and large strains [38, 39]. T3D2 element is used to model one-dimensional rebar assuming axial strain only. Fig. 9 depicts the discretization of the column.

The relationship between concrete and the rebars is assigned by an embedded region, where the rebars are the embedded substance, and the concrete is the host region. The steel bolsters are constrained as a rigid body to prevent their deformation during loading. The lower steel bolster is assigned as fixed support by preventing the translation in the three directions. The load is subjected to the upper bolster as implemented in experiments. The elements of all parts are seeded by a 20 mm size mesh in all orientations. The interaction between the steel bolsters and concrete column is selected to be a contact with the normal behavior of hard contact type to prevent penetration between them and allow separation after contact, and tangential behavior with a friction coefficient of 0.45 between concrete and steel. The friction coefficient between concrete and steel ranges between 0.29 to 0.6, as stated by Guo et al. [40], Rinker et al. [41], and Zhao and Zhu [42]. Friction coefficient sensitivity was checked by the software and chosen to be 0.45 throughout the numerical analysis due to the compressive stress considering the effect of a compressed rubber pad between concrete and steel. The analysis is carried out via a static general step.

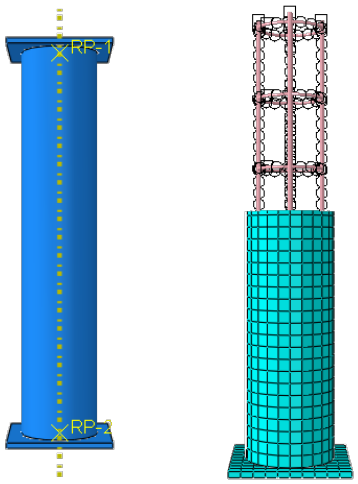

Fig. 9 Simulation and discretization of Column in Abaqus

4.2 Material models

The elastic behavior of concrete is described by its elastic modulus and Poisson's ratio. The plastic behavior of concrete is defined by the concrete damage plasticity (CDP) model to define different transition laws of strength under compression and tension [38, 39]. To represent the CDP model, the stress-inelastic strain of compression hardening - softening, and tensile stiffening, are determined according to the experimental results for compressive strength. Hognestad and Eurocode Eu-2004 [43] formula is adopted to capture the compressive stresses at the successive strains as follows:

$$\sigma_c = f_c^{'}\left[2\left(\frac{\varepsilon_o}{\varepsilon_{co}} - \left(\frac{\varepsilon_o}{\varepsilon_{co}}\right)^2\right)\right], \tag{1}$$

$$\varepsilon_{co} = \frac{2f_c^{'}}{E_c}, \tag{2}$$

$$E_c = 3320\sqrt{f_c^{'}} + 6900, \tag{3}$$

$$\varepsilon_o = \frac{0.4f_c^{'}}{E_c}, \tag{4}$$

$$\varepsilon_{pl.} = \varepsilon - \frac{\sigma_c}{E}, \tag{5}$$

$$d_c = 1 - \frac{\sigma_c}{f'c}, \tag{6}$$

where:

σ_c = Compressive stress at corresponding strain, MPa,
ε_{co} = Compressive strain at compressive strength,
ε_o = Strain at 40% of compressive strength (elastic limit),
E_c = Modulus of elasticity, MPa,
$\mathcal{E}_{pl}$ = Plastic strain, and d_c = damage parameter.

The yield tensile strength is considered (1/10–1/12) of compressive strength. Steel rebars are defined by the yield stresses for 5.1 mm bars and 8 mm bars as determined practically.

The surface failure of the finite elements is defined by the five parameters adopted in Abaqus, which are the dilation angle (ψ), eccentricity (Ɛ), the ratio of biaxial to uniaxial stress (f_{bo}/f_{co}), the shape of failure surface (K), and the viscosity parameter (μ). These values are listed in Table 4.

4.3 Model validation and analysis results

The implemented finite element model was validated by comparing it with the experimental data of the tested columns. To gauge the efficiency of the simulated model that predicts the structural behavior of columns, ultimate loads, longitudinal displacements, and crack patterns are compared with the experimental results.

4.3.1 Ultimate loads and longitudinal displacements

The FE loads compared to the experimental ones are illustrated in Fig. 10 for cracking and peak states. At the cracking state, the FE loads underestimate the experimental ones because the results of the analysis by Abaqus depend on the first crack stress, which is considered 0.4 of compressive strength. The relatively high cracking loads of the experimental results are due to the additional confinement of the concrete resulting from the basalt filaments in the concrete matrix in addition to steel ties. At peak state, the experimental loads are close to the numerical ones. The ratio of the FE loads to the experimental ones ranges between (1.0–1.09). The slight increase in numerical loads belongs to the high stiffness of concrete, as the numerical simulation of concrete does not contain voids, as is the case in the practical one.

Fig. 11 illustrates the numerical relationships between load and longitudinal displacement for all short columns. The columns show similarity in behavior until the initial cracking occurs. The load variation appears after that due to the effect of fibers on concrete strength, which provides confinement for the concrete and increases its tensile and compressive strength. The variation in displacement is due to the high stiffness shown by the numerical models for the same reason previously mentioned.

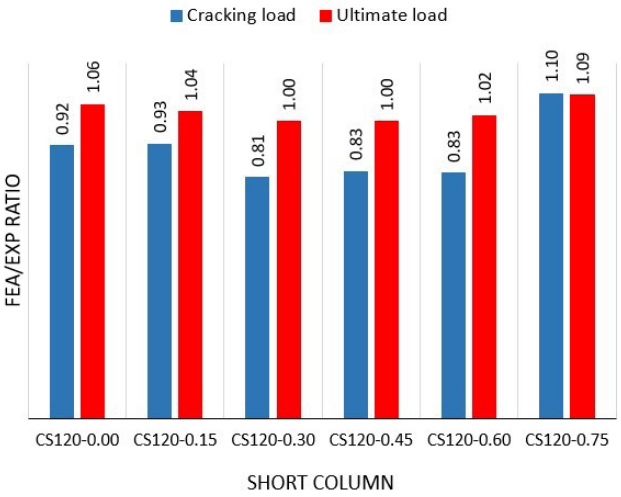

Fig. 10 The ratio of FEA to the experimental loads at cracking and the ultimate state

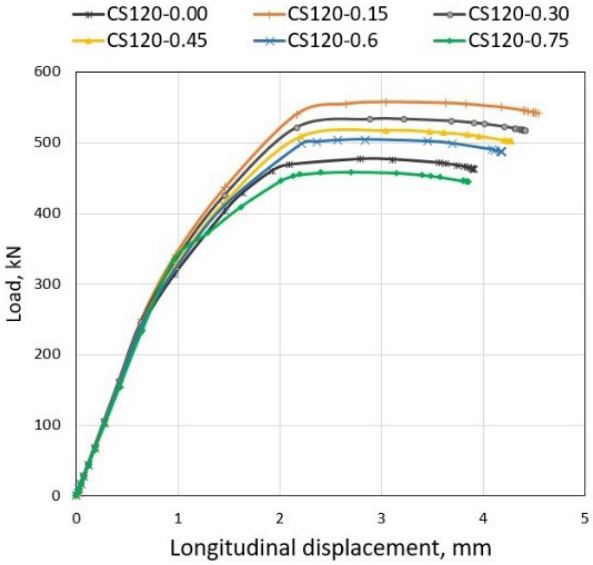

Fig. 11 Load versus longitudinal displacement of short columns

Table 4 The properties of materials used to simulate the short columns in Abaqus

Material	Properties					
Concrete	Elastic modulus, E_c MPa	Compressive strength, f_c', MPa		Tensile strength, f_t Pa		Poisson's ratio
	Variable, according to f_c'	According to the experiment results				0.18
	ψ	ε	f_{bo}/f_{co}	K	μ	
	25	0.1	1.16	0.67	1E-15	
Steel rebars	Diameter = 8 mm			Diameter = 5.1 mm		
	E_s	Yield stress	Poisson's ratio	E_s	Yield stress	Poisson's ratio
	200 GPa	563 MPa	0.30	200 GPa	563 MPa	0.30

At cracking loads for FEA, the longitudinal displacements for all columns are the same, where the ratio of FEA to experimental displacement ranges between (0.84–1.12). At the peak state, columns C120–0.30 and C120–0.15 show the highest displacement, respectively, as in the experimental results, followed by columns C120–0.45 and C120–0.60, as illustrated in Table 5.

4.3.2 Crack pattern

According to the numerical analysis, all columns failed in approximately the same pattern. The failure was due to concrete crushing.

Upon increasing loads, the cracks developed near the upper and lower supports and then extended to the lower third of the column. The cracks were concentrated on one side of the column at the maximum load that the column bear. The failure pattern of the FEA corresponded to the experimental results at the lower third of the columns, as illustrated in Fig. 12.

4.3.3 Steel rebar stress

At the maximum load, the longitudinal rebars did not yield for all columns, which indicates that the failure occurred because of the concrete fracture. However, the longitudinal rebars sustained (70–88)% of the yield stress at the maximum loads. The longitudinal rebars of column CS120-0.15 sustained the higher stress, while the column CS120-0.75 rebars sustained the lower stress, which corresponds to the experimental results.

Similarly, the transverse ties did not yield at the peak state for all columns. The middle tie sustained the highest stress, which is listed in Table 6. That indicated the tendency of the short column to buckle. Also, columns CS120-0.15 and CS120-0.30 recorded the highest stresses in the middle tie, while CS120-0.00 recorded the lowest value, which coincided with the maximum loads sustained by the columns, as shown in Fig. 13. Table 7 lists the stresses in the longitudinal bars and transverse ties.

4.3.4 Parametric study

Two additional parameters were numerically studied. The first one included changing the reinforcement ratio by using 6 mm, 8 mm, and 10 mm bar diameters to give 0.64%, 1.13%, and 1.78% reinforcement ratios, respectively. Test results are shown in Fig. 14. The results indicate that increasing the reinforcement ratio raised the load capacity of the columns. Alter the reinforcement ratio from 0.64% to 1.13% and 1.78% increased column loading capacity by about 7% and 14%, respectively. The results also showed that the stresses sustained by rebars did not reach yielding. Thus, the failure was due to crushing concrete before yielding rebars, as illustrated in Table 7.

Table 5 The longitudinal displacements at cracking and ultimate state for FEA and Experimental results

Column ID	Δ*cr*, mm		Δ*cr*	Δ*u*, mm		Δ*u*
	Exp.	FEA	FEA/EXP	Exp.	FEA	FEA/EXP
CS120-0.00	1.36	1.214	0.893	3.0	3.11	1.060
CS120-0.15	1.08	1.212	1.122	3.5	3.63	1.087
CS120-0.30	1.22	1.206	0.989	3.6	3.68	1.119
CS120-0.45	1.28	1.213	0.948	3.2	3.47	1.190
CS120-0.60	1.34	1.203	0.898	3.7	3.46	1.028
CS120-0.75	1.44	1.203	0.835	2.7	3.14	1.249

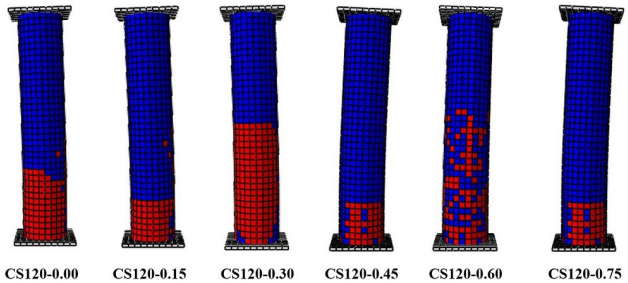

Fig. 12 Crack modes of the columns according to the FEA

Table 6 The ultimate loads and rebar stresses in the columns upon changing the reinforcement ratio

Column ID	Yield stress, *fy* = 563 MPa					
	db = 6 mm		*db* = 8 mm		*db* = 10 mm	
	Pu, kN	Rebar stress, MPa	*Pu*, kN	Rebar stress, MPa	*Pu*, kN	Rebar stress, MPa
CS120-0.00	443.3	401.7	476.80	406.9	509.7	353.3
CS120-0.15	521.3	443.4	557.62	493.3	595.9	404.6
CS120-0.30	498.1	435.0	533.39	457.0	567.1	377.6
CS120-0.45	473.8	428.0	517.69	440.2	526.1	337.3
CS120-0.60	470.0	409.5	504.37	440.9	537.5	371.5
CS120-0.75	425.3	391.7	458.87	401.5	458.4	294.9

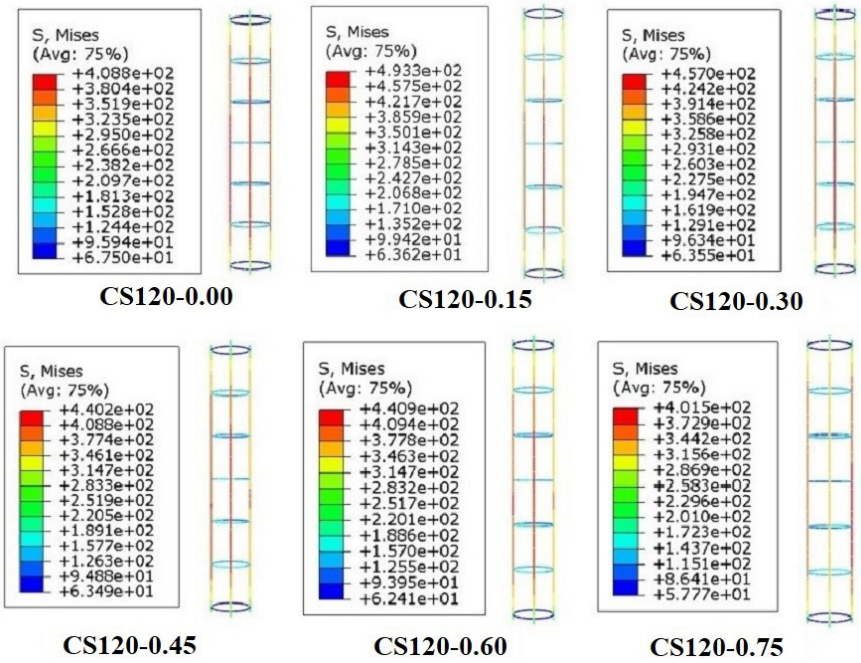

Fig. 13 The stresses sustained by the rebars of the short columns at maximum loading

Table 7 The stresses in the longitudinal bars and transverse ties of the columns

Column ID	Long. bar stress	Percentage of yield stress	Transverse Tie stress	Percentage of yield stress
CS120-0.00	408.8	0.726	124	0.315
CS120-0.15	493.3	0.876	171	0.434
CS120-0.30	457.0	0.812	195	0.495
CS120-0.45	440.2	0.782	189	0.480
CS120-0.60	440.9	0.783	188	0.477
CS120-0.75	401.5	0.713	172	0.437

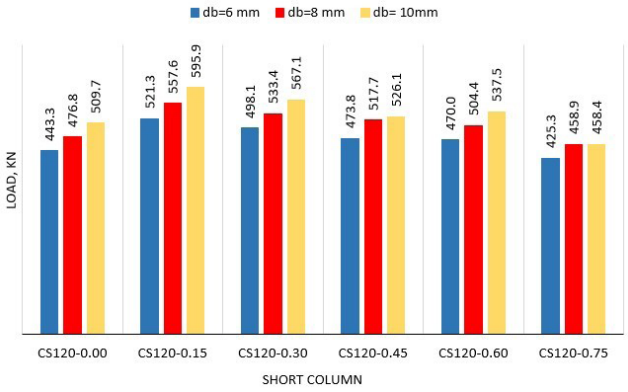

Fig. 14 The ultimate loads in columns for changing the reinforcement ratio

The second parameter was the variation of yielding stress of the rebar, while the diameter remained constant at 8 mm. Three yield stresses were adopted: 350 MPa, 450 MPa, and 563 MPa. The results showed that raising yield stress from 350 MPa to 450 MPa increases the load capacity by (1.0–2.8) % for all columns except CS120-0.00, where there was no change in ultimate load. However, altering yield stress from 450 to 563 MPa did not affect the maximum load because the stresses sustained by rebars remained under-yielding in both cases, as illustrated in Table 8.

Table 8 The ultimate loads and rebar stresses in the columns upon changing the yield stress

Column ID	Rebar diameter, db = 8 mm					
	fy = 350 MPa		fy = 450 MPa		fy =563 MPa	
	Pu, kN	Rebar stress, MPa	Pu, kN	Rebar stress, MPa	Pu, kN	Rebar stress, MPa
CS120-0.00	482.3	350.0	476.8	406.9	476,80	406.9
CS120-0.15	542.3	350.0	557.6	446.5	557.62	493.3
CS120-0.30	520.2	350.0	533.2	430.1	533.39	457.0
CS120-0.45	509.4	350.0	509.4	424.2	517.69	440.2
CS120-0.60	492.9	350.0	504.4	442.8	504.37	440.9
CS120-0.75	454.5	350.0	458.9	401.5	458.87	401.5

5 Conclusions

This research introduces experiments to investigate the impact of adding basalt fibers to the concrete matrix on the structural behavior of short circular columns. These effects include loading capacity, cracking load, crack pattern, and compressive strength of the concrete. Then, the short columns are numerically simulated by Abaqus software to investigate the stresses in longitudinal bars and transverse ties, besides testing two additional parameters: reinforcement ratios and yielding stresses. The following conclusions can derive:

Basalt filaments provide good internal confinement to the concrete, which can restrict early shrinkage, reduce the voids' number and size, and consequently enhance concrete strength.

Basalt fiber can enhance column ductility after the peak state. Therefore, it is significant in improving the structural behavior of short columns.

Increasing basalt fiber content up to 0.3% raises compressive strength. However, between (0.45–0.6)% volume fraction of basalt fiber, the increment of compressive strength decreases. The 0.75% caused reducing the compressive strength by 5.92%.

The influence of basalt fiber on small specimens is more pronounced than on larger ones.

Basalt fibers can delay the cracking of short columns and raise the loading capacity by about 50% more than conventional concrete columns at 0.6% and lower. The 0.15% and 0.3% volume fraction of basalt fiber awards the best loading capacity to the short columns. The 0.75% raised the cracking load slightly but reduced the ultimate bearing load.

Crushing concrete is the dominant failure in short concrete columns. The longitudinal rebars and transverse ties do not yield upon column failure. The middle tie sustained the highest stress.

Increasing the reinforcement ratio raised the loading capacity of the columns, whereas using rebars with lower yield stress reduces the maximum load.

References

[1] Iqbal, S., Ali, A., Holschemacher, K., Bier, T. A. "Mechanical properties of steel fiber reinforced high strength lightweight self-compacting concrete (SHLSCC)", Construction and Building Materials, 98, pp. 325–333, 2015. https://doi.org/10.1016/j.conbuildmat.2015.08.112

[2] Xin, H., Liu, Y., Mosallam, A. S., He, J., Du, A. "Evaluation on material behaviors of pultruded glass fiber reinforced polymer (GFRP) laminates", Composite Structures, 182, pp. 283–300, 2017. https://doi.org/10.1016/j.compstruct.2017.09.006

[3] Shaikh, F. U. A. "Review of mechanical properties of short fibre reinforced geopolymer composites", Construction and Building Materials, 43, pp. 37–49, 2013. https://doi.org/10.1016/j.conbuildmat.2013.01.026

[4] Hannawi, K., Bian, H., Prince-Agbodjan, W., Raghavan, B. "Effect of different types of fibers on the microstructure and the mechanical behavior of Ultra-High Performance Fiber-Reinforced Concretes", Composites Part B: Engineering, 86, pp. 214–220, 2016. https://doi.org/10.1016/j.compositesb.2015.09.059

[5] Alabduljabbar, H., Alyousef, R., Mohammadhosseini, H., Topper, T. "Bond behavior of cleaned corroded lap spliced beams repaired with carbon fiber reinforced polymer sheets and partial depth repairs", Crystals, 10(11), 1014, 2020. https://doi.org/10.3390/cryst10111014

[6] Dayyani, M., Mortezaei, A., Rouhanimanesh, M. S., Marnani, J. A. "Experimental Study on the Effect of Fibers on Engineered Cementitious Composite Short Square Columns", Periodica Polytechnica Civil Engineering, 66(3), pp. 798–808, 2022. https://doi.org/10.3311/PPci.19612

[7] Santarelli, M. L., Sbardella, F., Zuena, M., Tirillò, J., Sarasini, F. "Basalt fiber reinforced natural hydraulic lime mortars: A potential bio-based material for restoration", Materials and Design, 63, pp. 398–406, 2014. https://doi.org/10.1016/j.matdes.2014.06.041

[8] Ramesh, B., Eswari, S. "Mechanical behaviour of basalt fibre reinforced concrete: An experimental study", Materials Today: Proceedings, 43, pp. 2317–2322, 2020. https://doi.org/10.1016/j.matpr.2021.01.071

[9] Wang, X., He, J., Mosallam, A. S., Li, C., Xin, H. "The Effects of Fiber Length and Volume on Material Properties and Crack Resistance of Basalt Fiber Reinforced Concrete (BFRC)", Advances in Materials Science and Engineering, 2019, 7520549, 2019. https://doi.org/10.1155/2019/7520549

[10] Deák, T., Czigány, T. "Chemical Composition and Mechanical Properties of Basalt and Glass Fibers: A Comparison", Textile Research Journal, 79(7), pp. 645–651, 2009. https://doi.org/10.1177/0040517508095597

[11] Prince-Lund Engineering "Basalt Fiber Properties (2021 update)", 2011. [online] Available at: www.build-on-prince.com/basalt-fiber.html

[12] Basalt Fiber and Composite Materials, Technology Development "Basalt Continuous Fiber", [online] Available at: http://basaltm.com/en/bnv/basalt-continuous-fiber.html

[13] Li, Z., Ma, J., Ma, H., Xu, X. "Properties and Applications of Basalt Fiber and Its Composites", IOP Conference Series: Earth and Environmental Science, 186(2), 012052, 2018. https://doi.org/10.1088/1755-1315/186/2/012052

[14] Hirde, S., Shelar, S. "Effect of Basalt Fiber on Strength of Cement Concrete", International Journal of Current Engineering and Technology, 7(2), pp. 600–602, 2017.
[15] Branston, J., Das, S., Kenno, S. Y., Taylor, C. "Mechanical behaviour of basalt fibre reinforced concrete", Construction and Building Materials, 124, pp. 878–886, 2016. https://doi.org/10.1016/j.conbuildmat.2016.08.009
[16] Ayub, T., Shafiq, N., Nuruddin, M. F. "Mechanical properties of high-performance concrete reinforced with basalt fibers", Procedia Engineering, 77, pp. 131–139, 2014. https://doi.org/10.1016/j.proeng.2014.07.029
[17] Galen LLC "Basalt Chopped Fiber", 2009. [online] Available at: www.galencomposite.ru
[18] Liu, H., Liu, S., Wang, S., Gao, X., Gong, Y. "Effect of mix proportion parameters on behaviors of basalt fiber RPC based on Box-Behnken Model", Applied Sciences, 9(10), 2031, 2019. https://doi.org/10.3390/app9102031
[19] Borhan, T. M. "Thermal and Mechanical Properties of Basalt Fibre Reinforced Concrete", International Journal of Civil and Environmental Engineering, 7(4), pp. 334–337, 2013.
[20] Dias, D. P., Thaumaturgo, C. "Fracture toughness of geopolymeric concretes reinforced with basalt fibers", Cement and Concrete Composites, 27(1), pp. 49–54, 2005. https://doi.org/10.1016/j.cemconcomp.2004.02.044
[21] El-Din, H. K. S., Mohamed, H. A., El-Hak Khater, M. A., Ahmed, S. "Effect of Steel Fibers on Behavior of Ultra High Performance Concrete", presented at the First International Interactive Symposium on UHPC, Des Moines, IA, USA, July, 18–20, 2016. https://doi.org/10.21838/uhpc.2016.11
[22] El-Gelani, A. M., High, C. M., Rizkalla, S. H., Abdalla, E. A. "Effects of Basalt Fibres on Mechanical Properties of Concrete", MATEC Web of Conferences, 149, 01028, 2018. https://doi.org/10.1051/matecconf/201814901028
[23] Revade, A. B., Dharane, S. S. "Study the effects of short basalt fibers on mechanical properties of concrete", Journal of Civil Engineering and Environmental Technology, 13(3), pp. 1576–1580, 2015.
[24] Galishnikova, V. V., Chiadighikaobi, P. C., Emiri, D. A. "Comprehensive view on the ductility of basalt fiber reinforced concrete focus on lightweight expanded clay", Structural Mechanics of Engineering Constructions and Buildings, 15(5), pp. 360–366, 2019. https://doi.org/10.22363/1815-5235-2019-15-5-360-366
[25] Abdulhadi, M. "A comparative Study of Basalt and Polypropylene Fibers Reinforced Concrete on Compressive and Tensile Behavior", International Journal of Engineering Trends and Technology, 9(6), pp. 295–300, 2014. https://doi.org/10.14445/22315381/ijett-v9p258
[26] Krassowska, J., Kosior-Kazberuk, M. "Failure Mode of Basalt Fibre Reinforced Concrete Beams", IOP Conference Series: Materials Science and Engineering, 471, 052043, 2019. https://doi.org/10.1088/1757-899X/471/5/052043
[27] Algin, Z., Mermerdaş, K., Khalid, L. W. "Mechanical Performance of Basalt Fibre Reinforced Concretes", Journal of the Institute of Science and Technology, 10(2), pp. 1093–1106, 2020. https://doi.org/10.21597/jist.626757
[28] Al-Kharabsheh, B. N., Arbili, M. M., Majdi, A., Alogla, S. M., Hakamy, A., Ahmad, J., Deifalla, A. F. "Basalt Fibers Reinforced Concrete: Strength and Failure Modes", Materials, 15(20), 7350, 2022. https://doi.org/10.3390/ma15207350
[29] Shamass, R., Hakimi, A. U., Limbachiya, V. "Impact of Chopped Basalt Fibres on the Mechanical Properties", In: 3rd Conference on Sustainability in Civil Engineering (CSCE'21), Islamabad, Pakistan, 2021, pp. 17–23. ISBN: 978-969-23344-2-6
[30] Meyyappan, P. L., Carmichael, M. J. "Studies on strength properties of basalt fibre reinforced concrete", Materials Today: Proceedings, 43, pp. 2105–2108, 2020. https://doi.org/10.1016/j.matpr.2020.11.890
[31] Wang, C.-K., Salmon, C. G., Pincheira, J. A. "Reinforced Concrete Design", (7th ed.), John Wiley & Sons, 2007. ISBN: 978-0-471-26286-2
[32] Jabbar, A. M., Hamood, M. J., Mohammed, D. H. "The effect of using basalt fibers compared to steel fibers on the shear behavior of ultra-high performance concrete T-beam", Case Studies in Construction Materials, 15, e00702, 2021. https://doi.org/10.1016/j.cscm.2021.e00702
[33] Wang, J., Zhang, Y. "Experimental research on mechanical and working properties of non-dipping chopped basalt fiber reinforced concrete", In: Proceedings of the 3rd International Conference on Information Management, Innovation Management and Industrial Engineering, Kunming, China, 2010, pp. 635–637. ISBN: 978-1-4244-8829-2 https://doi.org/10.1109/ICIII.2010.633
[34] Wang, X., Yang, Y., Yang, R., Liu, P. "Experimental Analysis of Bearing Capacity of Basalt Fiber Reinforced Concrete Short Columns under Axial Compression", Coatings, 12(5), 654, 2022. https://doi.org/10.3390/coatings12050654
[35] Wang, X., Li, C., Zhou, W., Xie, H. "Experimental Study on the Axial Compression of Short Basalt Fiber Reinforced Concrete Columns with Spiral Stirrups", Journal of Engineering Science and Technology Review, 10(1), pp. 55–60, 2017. https://doi.org/10.25103/JESTR.101.09
[36] ACI Committee 318 "318-19(22): Building Code Requirements for Concrete and Commentary", American Concrete Institute, Farmington Hills, MI, USA, 2019. https://doi.org/10.14359/51716937
[37] Sika, "Sika® ViscoCrete ® -180 G", 2020. [online] Available at: https://www.sika.com/
[38] Simulia, Dassault Systèmes "Getting Started with Abaqus: Interactive Edition", (v. 6.12), 2012. [online] Available at: http://dsk-016-1.fsid.cvut.cz:2080/v6.12/books/gsa/default.htm?startat=ch01s02.html
[39] Solhmirzaei, R., Kodur, V. K. R. "Modeling the response of ultra high performance fiber reinforced concrete beams", Procedia Engineering, 210, pp. 211–219, 2017. https://doi.org/10.1016/j.proeng.2017.11.068
[40] Guo, Q., Chen, Q., Xing, Y., Xu, Y., Zhu, Y. "Experimental Study of Friction Resistance between Steel and Concrete in Prefabricated Composite Beam with High-Strength Frictional Bolt", Advanced in Materials Science and Engineering, 2020, 1292513, 2020. https://doi.org/10.1155/2020/1292513

[41] Rinker, M. W., Pilli, S. P., Karri, N. K., Deibler, J. E., Johnson, K. I., Holbery, J. D., Mullen, O. D., Hurley, D. E. "Structural Integrity of Single Shell Tanks at Hanford - 9491", presented at WM2009 Conference, Phoenix, AZ, USA, March, 1–5, 2009.

[42] Zhao, W., Zhu, B. "Theoretical model for the bond-slip relationship between ribbed steel bar and confined concrete", Structural Concrete, 19(2), pp. 548–558, 2018. https://doi.org/10.1002/suco.201700008

[43] Technical Committee CEN/TC250 "Eurocode 2: Design of concrete structures - Part 1-2: General rules -Structural fire design", European Committee for Standardization, Brussels, Belgium, 2011. [online] Available at: https://eurocodes.jrc.ec.europa.eu/EN-Eurocodes/eurocode-2-design-concrete-structures